Journal of Technology Research (JTR)
Volume 3, Special Issue, (2025), pp 770-779 ISSN 3005-639X
The 7th Conference of Engineering Sciences and Technology
(CEST-2025)

# A Comparative Study of Neural Network Algorithms for Modelling Hydrogen Sulphide Removal from Natural Gas

Mohamed Baqar[1*], Rayan Alzeyani[1], Montaha Zraig[1], Retaj Madi[1]

[1]Department of Chemical Engineering, Faculty of Engineering, University of Tripoli, Tripoli, Libya.

*Corresponding author email: m.baqar@uot.edu.ly

Received: 13-10-2025 | Accepted: 02-12-2025 | Available online: 25-12-2025 | DOI:10.26629/jtr.2025.72

**ABSTRACT**

This study focuses on the prediction of hydrogen sulphide removal efficiency in natural gas sweetening processes using Artificial Neural Networks (ANN). The developed model was trained on experimental solubility data that were extracted from literature for 17 different absorbents at various operating conditions, with a total of 470 data points. Three training algorithms of Scaled Conjugate Gradient (SCG), Levenberg Marquardt (LM), and Bayesian Regularization (BR) were evaluated to determine the optimal ANN architecture. The performance of each model was assessed using mean squared error (MSE) and the coefficient of determination ($R^2$). The SCG algorithm achieved its best performance at 35 hidden neurons, with MSE = 0.0183 and $R^2$ = 0.8799, showing gradual improvements but lower accuracy compared to other methods. The LM algorithm performed optimally at 15 hidden neurons, yielding MSE = 0.002865 and $R^2$ = 0.9785, demonstrating excellent predictive accuracy. The BR algorithm outperformed both SCG and LM, with the best results at 25 hidden neurons, achieving MSE = 0.001465 and $R^2$ = 0.9904, indicating superior generalization and stability. These results highlight the potential of ANN as a robust tool for simulating gas sweetening processes and supporting industrial decision-making.

**Keywords:** Artificial Neural Networks; Hydrogen Sulphide Removal; Gas Sweetening.

# دراسة مقارنة لخوارزميات الشبكات العصبية في نمذجة إزالة كبريتيد الهيدروجين من الغاز الطبيعي

محمد بقر[1]، ريان الزياني[1]، منتهى زريق[1]، رتاج مادي[1]

[1]قسم الهندسة الكيميائية ، كلية الهندسة ، جامعة طرابلس ، مدينة طرابلس، دولة ليبيا.

**ملخـــــص البحـــــث**

تركز هذه الدراسة على تطبيق الشبكات العصبية الاصطناعية **(ANN)** للتنبؤ بكفاءة إزالة كبريتيد الهيدروجين **($H_2S$)** في عمليات تطييع الغاز الطبيعي. النموذج المقترح تم تدريبه على نتائج دوبانية تجريبية اخذت من دراسات سابقة لعدد 17 مادة مازة عند ظروف تشغيلية مختلفة، لتنتج عدد 470 نقطة. تم تقييم ثلاث خوارزميات تدريب وهي: التدرج المترافق المعياري **(SCG)**، وليفينبرغ–ماركاردت **(LM)**، والتنظيم البايزي **(BR)** لتحديد البنية المثلى للشبكة العصبية الاصطناعية. تم تقييم أداء كل نموذج بناءً على متوسط الخطأ التربيعي **(MSE)** ومعامل التحديد **($R^2$)**. حققت خوارزمية **(SCG)** أفضل أداء لها عند 35 عصبونًا خفيًا (**$R^2$= 0.8799**، **MSE= 0.0183**)، حيث أظهرت تحسناً تدريجياً لكن بدقة أقل مقارنة بالطرق الأخرى. بينما أدت خوارزمية **(LM)** أفضل أداء عند 15 عصبونًا

خفيًا (0.9785 = $R^2$، **0.002865 =MSE** )، مما يُظهر دقة تنبؤية عالية. وتفوقت خوارزمية (**BR**) على الخوارزميتين السابقتين، حيث حققت أفضل النتائج عند 25 عصبونًا خفيًا (0.9904 = $R^2$، **0.001465 =MSE** )، مما يشير إلى قدرة استقرائية واستقرارية فائقة. تُسلط هذه النتائج الضوء على إمكانات الشبكات العصبية الاصطناعية كأداة قوية لمحاكاة عمليات تطييع الغاز ودعم اتخاذ القرارات الصناعية.

**الكلمات الدالة:** الشبكات العصبية الاصطناعية، إزالة كبريتيد الهيدروجين، تطييع الغاز.

## 1. INTRODUCTION

The removal of hydrogen sulphide ($H_2S$) from natural gas is a critical step in gas purification due to the compound's toxicity, corrosiveness, and environmental impact. Depending on gas composition, pressure, and $H_2S$ concentration, different industrial processes are used to ensure effective removal. The most common processes include; amine gas treating (gas sweetening), claus process, iron sponge process, adsorption process, membrane separation, and biological desulfurization [1,2]. However, among the various methods available for $H_2S$ removal, amine gas sweetening (shown in **Figure 1**) is one of the most widely applied and effective technologies in the natural gas industry [3]. The figure shows that sour feed gas is fed into the amine unit. The aqueous amine solution enters at the top of the amine absorber unit, and the sour gas is then fed into the bottom, flowing counter-currently while in contact with it. The amine solution that absorbed the acid gas emerged from the bottom of the absorber as the rich amine. Sweet gas that has been treated leaves at the absorber's top. Therefore, it can be postulated that amines remove $H_2S$ in a two-step process, where the gas dissolves in the liquid (physical absorption) and then the dissolved gas dissociates into a weak ionic acid, reacts with the weakly basic amines [4]. Several types of amines have been studied such as monoethanolamine (MEA), diethanolamine (DEA), methyldiethanolamine (MDEA), and sterically hindered amines like 2-amino-2-methyl-1-propanol (AMP) and tert-butyl ethanolamine (TBEE) [4]. These solvents react reversibly with acidic gases, which make them widely used in gas sweetening units. For example, MDEA is characterized by different reaction rates of $H_2S$ and of carbon dioxide ($CO_2$) in the solution; those of $H_2S$ are instantaneous, while those of $CO_2$ are finite and slow with respect to the mass transfer rate [5]. This difference in the reaction rate makes the MDEA absorption system kinetically selective towards $H_2S$, so it is used for purification of several gaseous streams, in particular when both the two acid gases are present [4].

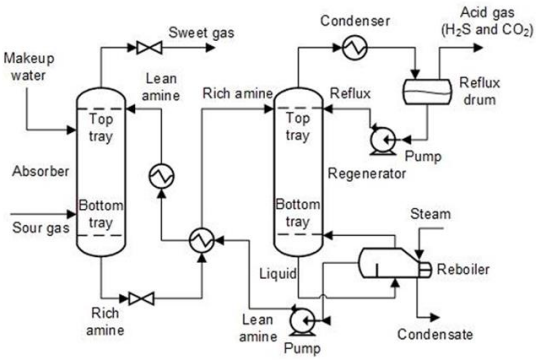


**Fig 1.** Typical process flow diagram of an amine - treating unit for $H_2S$ removal [6].

Inspired by the human brain, Artificial Neural Networks (ANNs) are advanced computational models designed to detect complex patterns in data. Their key strengths, compared to traditional models, are their ability to model non-linear relationships and handle noisy data, making them powerful tools for difficult engineering problems and universal function approximators [7]. The ANN's structure consisting of input, hidden, and output layers of interconnected neurons that are capable of processes information through activation functions, enabling it to learn sophisticated

mappings between inputs and outputs for tasks like prediction and classification [8].

Several studies have demonstrated the effectiveness of artificial intelligence specifically neural network models in predicting the solubility and concentration of $H_2S$ during gas sweetening processes [9,10]. Nimmanterdwong *et al.* [11] developed an ANN model to predict $H_2S$ solubility in various absorbents, including amines, ionic liquids, and hybrid mixtures. The study found that Levenberg–Marquardt achieved the best performance (MSE = 0.0014, $R^2$ = 0.9817). Hakimi *et al.* [6] applied ANN to predict $H_2S$ concentration in sweet gas exiting an Acid Gas Removal Unit (AGRU). The model used input variables such as MDEA and Piperazine concentrations, temperature, and pressure. The study showed that the best-performing ANN trained via Levenberg–Marquardt technique achieved ($R^2$ = 0.966, MAE = 0.066, and RMSE = 0.122). Shafiei *et al.* [12] investigated $H_2S$ solubility in ionic liquids using machine learning techniques. Additionally, the compared traditional backpropagation ANN (BP-ANN) with particle swarm optimization-trained ANN (PSO-ANN) yielding $R^2$ = 0.9515 and MSE = 0.00335 for BP-ANN, while PSO-ANN achieved significantly better performance with $R^2$ = 0.9922 and MSE = 0.00025. Therefore, it is clear that ANN provide a promising solution, as they can capture hidden patterns in the data and predict system behavior accurately and efficiently.

Therefore, selecting the optimal model is challenging due to the availability of several training algorithms and network configurations. This necessitates a thorough performance evaluation to identify the best model for a specific application.

In this study, three training algorithms (SCG, LM, and BR) were tested to evaluate their performance in predicting the behavior of the $H_2S$ removal unit. Furthermore, the results based on performance metrics such as MSE and $R^2$ were compared to identify the most accurate and reliable model [13]. Then the best model was selected for a comprehensive analysis of its performance using illustrative MATLAB plots.

## 2. MATERIALS AND METHODS

MATLAB, a popular tool for data analysis and algorithm development, was used in this project to create an ANN model for predicting $H_2S$ solubility in various absorbents. The model is based on the experimental solubility data of $H_2S$ in various absorbents. The developed model was trained on experimental solubility data that were extracted from published literature [14-19] for 17 different absorbents at various operating conditions, in a total of 470 data points as depicted in **Appendix A**. . The absorbents include amines, ionic liquids, physical organic solvents, and hybrid absorbents (such as amine, physical solvent and amine, and ionic liquid), providing a diverse and comprehensive dataset suitable for training the ANN model.

In this study, the solubility of $H_2S$ was considered as the output, while the absorbents and their weight fractions as well as operating temperature (K) and pressure (kPa) were considered as inputs as depicted in **Figure 2**. In case of a pure absorbent, unity weight fraction was the input as the absorbent concentration. For a blended absorbent, the weight fraction of each absorbent and its corresponding absorbent codename were chosen as the input into the ANN model. The total of 470 data points was split into three sets with 70% for training, and the remaining 30% was divided equally into validation and testing sets with each representing 15% of the total data.

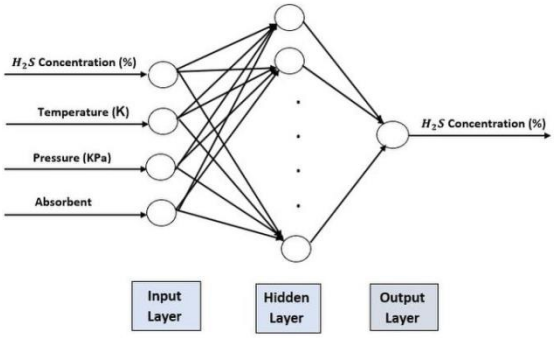


**Fig 2.** The configured artificial neural network with multiple layers.

## 3. THEORY AND CALCULATION

### *3.1. Mathematical expressions*

Due to the slightly disparate scales of the different variables in the dataset, a min-max normalization approach was applied to the training data to bring all features to the same scale.

$$\hat{x} = \frac{X - X_{min}}{X_{\max} - X_{min}} \quad (1)$$

where:
$\hat{x}$ is the normalized value.
x is the original input value.
$x_{min}$ is the minimum value.
$x_{max}$ is the maximum value.

The Neural Networks Toolbox in MATLAB with Neural Fitting Application was applied for designing the ANN model.

The model employs the backpropogation (BP) framework within the multilayer, feedforward (FF) architecture, a powerful pattern that enables the network to adapt by minimizing error through gradient decent. The equation that expresses the weight update process during training is given by:

$$\omega_{ij\,(t+1)} = \omega_{ij(t)} + \eta\delta_j x_i \quad (2)$$

Where:
$w_{ij}$ is the weight between neuron i and neuron j
$\delta_j$ is the error term for neuron j
$x_i$ is the input from neuron i
$\eta$ is the learning rate

The FF structure, typically comprising hidden layers of sigmoid neurons and a linear output layer, is capable of modeling complex linear and nonlinear relationships. As no single BP based algorithm is optimal, the performance are highly dependent on the specific problem and data. Therefore, the strategy of this research is to evaluate three distinct and efficient algorithm: Levenberg-Marquardt (TRAINLM), as of its rapid convergence; Scaled Conjugate Gradient (TRAINSCG), as of its robustness and lack of line search parameters; and Bayesian Regularization (TRAINBR), as of its ability to improve generalization and prevent overfitting. The performance of these algorithms will be compared using MSE and $R^2$ to identify the most effective training strategy for the $H_2S$ solubility prediction.

### 3.2. *Training the neural network*

A range of hidden neuron counts, from 1 to 35, is tested in order to determine the optimal network architecture. After constructing the neural network, the input data are fed into the network along with the desired outputs. The network adapts to the data through a process known as training, using specific training algorithms. These algorithms determine the modelling, learning, and validation properties of the network.

In this study, the activation function employed in the hidden layer is the hyperbolic tangent sigmoid transfer function (tansig), which is a widely used activation function for hidden layers in neural networks, is given by:

$$f(x) = \frac{2}{1+e^{-2x}} - 1 \quad (3)$$

### *3.3. Model evaluation*

To evaluate a prediction performance of the developed ANN models, an error analysis through the MSE and $R^2$ was conducted. **Figure 3** summarizes the steps applied for evaluation. These two parameters are typically used for indicating an error between the actual and predicted values (in this case, the experimental and the predicted solubility of $H_2S$). Equations

used for calculations of the two predictive indicators (MSE and $R^2$) are given by equations (4) and (5), respectively [13].

$$MSE = \frac{\sum_{i=1}^{n}(\alpha_{\exp i} - \alpha_{pred\ i})^2}{n} \quad (4)$$

$$\boldsymbol{R^2} = 1 - \left(\frac{\sum_{i=1}^{n}(\alpha_{pred\ i} - \alpha_{exp\ i})^2}{\sum_{i=1}^{n}\left(\alpha_{exp\ i} - \alpha_{exp\ i}^{-}\right)^2}\right) \quad (5)$$

Where:

n is the number of data points.

$\alpha_{\exp i}$ is experimental solubility of $H_2S$.

$\alpha_{pred\ i}$ is predicted solubility of $H_2S$.

$\alpha_{exp}^{-}$ is average experimental solubility of $H_2S$.

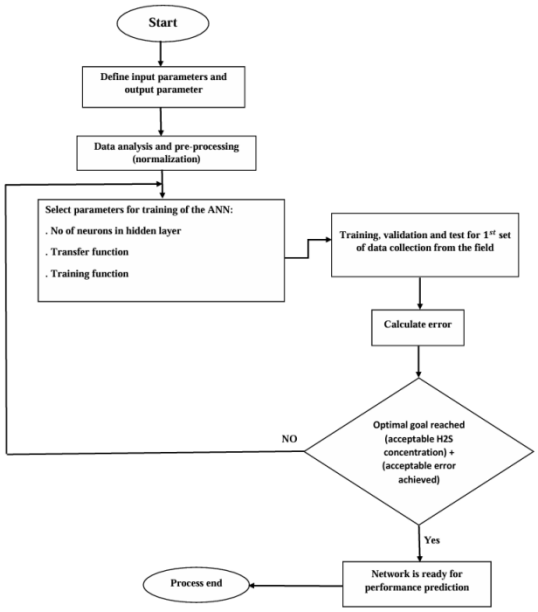


**Fig 3.** Flowchart summarizing the steps applied.

Additionally, instead of individually comparing the predicted and experimental data in a tabulation format, the parity chart positions predicted solubility of $H_2S$ with its corresponding experimental value in a graphical format. Along the diagonal line, where the predicted value equals to the experimental value, each coordination of the predicted and experimental values is located accordingly. For a promising ANN model, the data distribution should be closely along the diagonal line.

## 4. RESULTS AND DISCUSSION

### *4.1. Performance of the selected ANN model*

The evaluation metrics were calculated for the training, validation, and testing datasets for the LM-ANN and SCG-ANN models. However, the BR-ANN model utilized only training and testing datasets. This is attributed to the fundamental difference in the BR training algorithm. Unlike LM and SCG, which uses a separate validation set for early stopping to prevent overfitting, BR uses a probabilistic framework that intrinsically penalizes model complexity. This is achieved by minimizing an objective function that balances data error with a regularization term based on the magnitude of the network weights [11,20,21].

As a result, three predictive models of LM-ANN, BR-ANN, and SCG-ANN were constructed. To justify the effectiveness of the developed models, the MSE and $R^2$ were applied as depicted in **Figures 4** and **5**, respectively.

The results for the SCG algorithm show a gradual improvement in both the MSE and $R^2$ with an increasing number of neurons, reaching the best performance on the testing set at 35 hidden neurons, where MSE(test) = 0.018344 and $R^2$(test) = 0.8799. For example, a consistent improvement in performance across the training, validation, and testing sets, particularly beyond 20 neurons, where MSE values drop noticeably and $R^2$ steadily approaches 0.80–0.88. The gap between training, validation, and testing performance remains relatively small, suggesting good generalization capability. It is also notable that this small performance gap persists at higher neuron counts, indicating that the model does not exhibit strong overfitting at 35 neurons; all datasets show relatively similar behavior. However, the relatively higher MSE on the testing set compared to some other algorithms indicates that SCG may not provide the highest possible prediction accuracy, but it achieves a reasonable balance between complexity and training stability.

The figures also show the performance of the LM algorithm which shows a rapid improvement in accuracy as the number of hidden layer neurons increases, with a substantial drop in the MSE occurring between 5 and 10 neurons. The optimal configuration was achieved with 15 hidden neurons, resulting in MSE(test) = 0.002865 and $R^2$(test) = 0.9785, indicating excellent predictive capability. Up to around 30 neurons, both MSE and $R^2$ remain stable and consistently high in performance, with low error and $R^2$ values close to 1.0 across training, validation, and testing sets. However, after exceeding 30 hidden neurons, there is a noticeable increase in MSE and a slight drop in $R^2$, especially in the validation and testing datasets. This behavior suggests that the model begins to lose generalization capacity, possibly due to overfitting caused by excessive network complexity. The gap between the training and testing curves remains relatively small in the optimal range (around 15 neurons), indicating stable learning and minimal overfitting. The $R^2$ value of approximately 0.98 in the optimal configuration means the model explains about 98% of the variance in the target variable on unseen data as an excellent result.

The figures also show the performance of the BR algorithm which demonstrates rapid and consistent performance improvement as the number of hidden neurons increases, with a sharp decline in MSE and a steady rise in the $R^2$. The optimal configuration was achieved with 25 hidden neurons, yielding an MSE(test) = 0.001465 and $R^2$(test) = 0.9904, indicating excellent predictive accuracy and minimal generalization error. Compared to SCG and LM, BR achieves high accuracy with fewer neurons while maintaining exceptional stability across both training and testing datasets. Notably, after around 10 neurons, the performance curves flatten, with only marginal gains observed beyond this point. The minimal gap between training and testing results suggests strong resistance to overfitting. While BR maintains superior stability, slight fluctuations in MSE are observed when increasing the hidden neurons beyond 25, accompanied by negligible changes in $R^2$. This indicates that increasing complexity past the optimal point offers no significant benefit and may introduce unnecessary computational overhead.

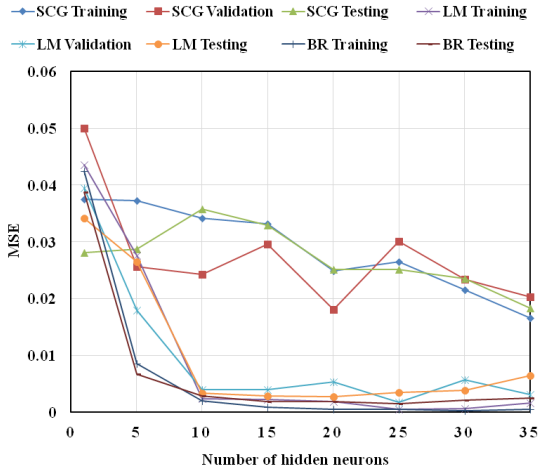


**Fig 4.** MSE of the three developed ANN models at various numbers of hidden neurons.

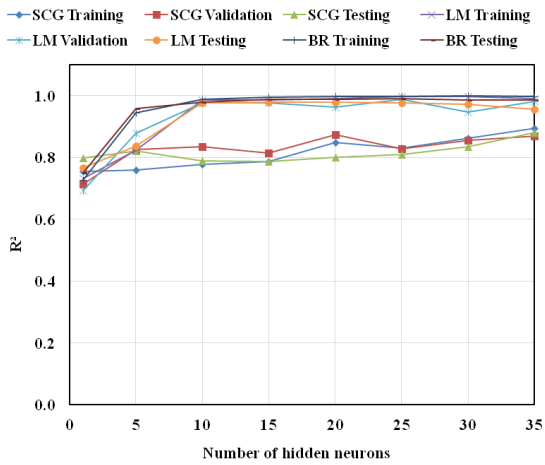


**Fig 5.** $R^2$ of the three developed ANN models at various numbers of hidden neurons.

Additionally, **Table 1** shows summarized results of the optimal hidden neuron configuration, MSE, and $R^2$ for each training algorithm. Among the tested models, the number of; input neurons of 4, output neurons of 1, and hidden layer of 25 neurons, for the 470 data points of experimental $H_2S$ solubility data that were extracted from published literature [14-19], BR achieved the best overall results,

with the lowest MSE (0.001465) and the highest $R^2$ (0.9904), indicating excellent predictive accuracy and minimal generalization error. LM followed closely, reaching its optimal performance at 15 hidden neurons with an MSE of 0.002865 and $R^2$ of 0.9785, providing high accuracy with relatively low network complexity. SCG showed the lowest performance in terms of prediction accuracy, achieving its best results at 35 hidden neurons with an MSE of 0.018344 and $R^2$ of 0.8799, although it demonstrated stable learning behavior without significant overfitting. LM also offers excellent performance with faster convergence, making it an efficient alternative when computational time is a priority. SCG, while less accurate, may still be considered when robustness and training stability are the main concerns.

**Table 1.** MSE, $R^2$, and the number of hidden neurons of the three optimized ANN models.

| ANN model | Number of hidden neurons | MSE(test) | $R^2$(test) |
|---|---|---|---|
| BR- ANN | 25 | 0.001465 | 0.9904 |
| LM-ANN | 15 | 0.002865 | 0.9785 |
| SCG-ANN | 35 | 0.018344 | 0.8799 |

### *4.2. Evaluation of the selected ANN model*

**Figure 6** shows the number of; input neurons of 4, output neurons of 1, and hidden layer of 25 neurons, for the 470 data points of the experimental $H_2S$ solubility data at various operating conditions. This structure was selected as the final model. The training was performed using the BR algorithm to achieve high accuracy and robust generalization.

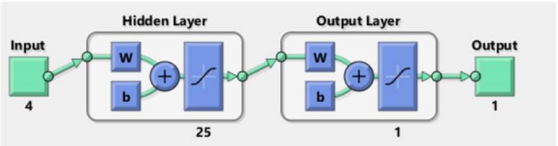


**Fig 6.** The obtained optimum structure of ANN architecture for prediction of $H_2S$ output concentration.

**Figure 7** depicts the regression plot, illustrating the relationship between the network outputs and the actual target values for the training set (R = 0.99854), testing set (R = 0.99551), and all data combined (R = 0.9979). These values indicate excellent accuracy and predictive capability of the selected model, confirming its effectiveness in representing the target data.

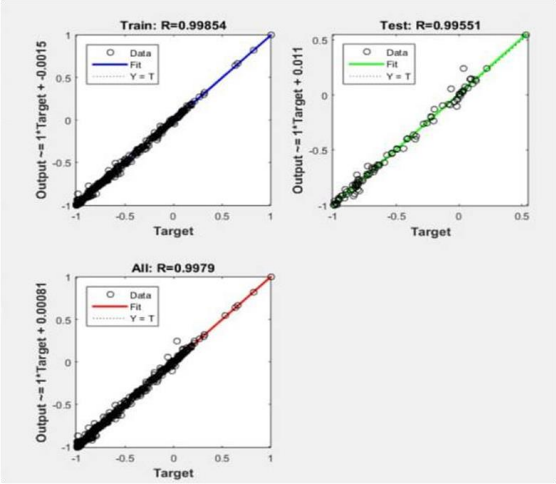


**Fig 7.** Parity plots of the optimized BR-ANN model for training data (top left), testing data (top right), and all data (bottom).

### *4.3. Interpretation of the ANN model results*

The high accuracy of the developed models indicates that it has effectively learned the underlying continuous relationship described by principles such as Henry's law at lower pressures and more complex interactions that dominate at higher pressures without requiring arbitrary data segmentation.

#### *4.3.1. Non ideal solubility behavior*

Unlike simple linear models, the developed ANN model captures the non ideal behavior of $H_2S$ solubility. This include deviations from Henry's law at moderate to high pressures where the increase in solubility is not linear with pressure. The model also predicts the curved isotherm and plateaue resulting from factors such as gas-phase non ideality and liquid-phase molecular interactions. Additionally, in a mixed solvent system such as amine blends, the ANN model accounts for the competition between $H_2S$ and other components for solvation sites.

### *4.3.2. The interaction effects*

The solubility at a given pressure is not a single value, rather it is a function of other conditions. This suggests that the ANN model integrates the effect of pressure with variations in solvent concentration such as MDEA where the higher pressure might allow for the use of slightly leaner solvent to achieve the same outlet $H_2S$ specification which is critical for process optimization.

### *4.3.3. Implications of the model*

The high predictive accuracy of the developed model across a continuous pressure range makes it a powerful tool for process design and real time optimization. It enables engineers to simulate $H_2S$ solubility over entire operating range, which is important for optimizing gas process plant such as adjusting solvent rates, compressor discharge pressures in response to changing feed conditions.

## 5. CONCLUSIONS

The ANN models for the prediction of $H_2S$ solubility were successfully developed and trained using three different algorithms: SCG, LM, and BR. The model performance was assessed using MSE and $R^2$. The results showed that the BR-ANN model provided the best predictive performance with an optimal configuration of 25 hidden neurons, achieving (MSE = 0.001465 and $R^2$ = 0.9904), reflecting excellent accuracy and generalization. The LM-ANN model achieving strong results with 15 hidden neurons (MSE = 0.002865, $R^2$ = 0.9785), making it a reliable alternative with faster convergence. The SCG-ANN model, although stable and less prone to overfitting, achieved lower prediction accuracy with its best configuration at 35 hidden neurons (MSE = 0.018344, $R^2$ = 0.8799). The high accuracy of the BR-ANN model does not merely provide a numerical fit; it serves as a high fidelity data driven surrogate for the complex thermodynamic equilibrium of the $H_2S$ solvent system. Its low MSE and high $R^2$ all over a continuous pressure range confirm its capability as a predictive tool that respects the underlying chemical engineering principles, making it directly applicable for complicated design and real-time optimization tasks in gas processing plants. Despite these promising results, the model accuracy may diminish if applied to processes operating under conditions outside the training data.

## 6. ACKNOWLEDGMENT

The authors would like to thank the Department of Chemical Engineering, University of Tripoli for their support.

## REFERENCES

[1] Kohl, A.; Nielsen, R., Gas purification 5th ed. *Houston: Gulf Publishing Company* **1997**

[2] Cavaignac, R. S.; Ferreira, N. L.; Guardani, R., Techno-economic and environmental process evaluation of biogas upgrading via amine scrubbing. *Renewable Energy* **2021,** *171*, 868-880

[3] Agarwal, N.; Cao Nhien, L.; Lee, M., Rate-based modeling and assessment of an amine-based acid gas removal process through a comprehensive solvent selection procedure. *Energies* **2022,** *15* (18), 6817.

[4] Esmaeili, A.; Yoon, T.; Atsbha, T. A.; Lee, C.-J., Rate-based modeling and energy optimization of acid gas removal from natural gas stream using various amine solutions. *Process Safety and Environmental Protection* **2023,** *177*, 643-663.

[5] Versteeg, G.; van Swaaij, W. P. M., On the kinetics between $CO_2$ and alkanolamines both in aqueous and non-aqueous solutions—II. Tertiary amines. *Chemical engineering science* **1988,** *43* (3), 587-591.

[6] Hakimi, M.; Omar, M. B.; Ibrahim, R., Application of neural network in predicting $H_2S$ from an acid gas removal unit (AGRU) with different compositions of solvents. *Sensors* **2023,** *23* (2), 1020.

[7] Grznar, J.; Prasad, S.; Tata, J., Neural networks and organizational systems: Modeling non-linear relationships. *European Journal of Operational Research* **2007,** *181* (2), 939-955.

[8] Soyer, M. A.; Tüzün, N.; Karakaş, Ö.; Berto, F., An investigation of artificial neural network structure and its effects on the estimation of the low-cycle fatigue parameters of various steels. *Fatigue & Fracture of Engineering Materials*

*& Structures* **2023,** *46* (8), 2929-2948.

[9] Alardhi, S. M.; Al-Jadir, T.; Hasan, A. M.; Jaber, A. A.; Al Saedi, L. M., Design of artificial neural network for prediction of hydrogen sulfide and carbon dioxide concentrations in a natural gas sweetening plant. *Ecological Engineering & Environmental Technology* **2023,** *24*.

[10] He, Y.; Yang, A.; Zou, C.; Fan, T.; Lan, Q.; He, Y.; Wang, M.; Sunarso, J.; Kong, Z. Y., An interpretable surrogate model for H2S solubility forecasting in ionic liquids based on machine learning. *Separation and Purification Technology* **2025,** *357*, 130061.

[11] Nimmanterdwong, P.; Changpun, R.; Janthboon, P.; Nakrak, S.; Gao, H.; Liang, Z.; Tontiwachwuthikul, P.; Sema, T., Applied artificial neural network for hydrogen sulfide solubility in natural gas purification. *ACS omega* **2021,** *6* (46), 31321-31329.

[12] Shafiei, A.; Ahmadi, M. A.; Zaheri, S. H.; Baghban, A.; Amirfakhrian, A.; Soleimani, R., Estimating hydrogen sulfide solubility in ionic liquids using a machine learning approach. *The Journal of Supercritical Fluids* **2014,** *95*, 525-534.

[13] Montgomery, D. C., Peck, E. A., Vining, G. G. (**2012**). Introduction to Linear Regression Analysis (5th ed.). John Wiley & Sons.

[14] Jou, F. Y.; Carroll, J. J.; Mather, A. E.; Otto, F. D., The solubility of carbon dioxide and hydrogen sulfide in a 35 wt% aqueous solution of methyldiethanolamine. *The Canadian Journal of Chemical Engineering* **1993,** *71* (2), 264-268.

[15] Macgregor, R. J.; Mather, A. E., Equilibrium solubility of $H_2S$ and $CO_2$ and their mixtures in a mixed solvent. *The Canadian Journal of Chemical Engineering* **1991,** *69* (6), 1357-1366.

[16] Gonzalez Tovar, K.; Afonso, R.; Stringari, P.; Coquelet, C.; Cloarec, E.; Cadours, R.; de Meyer, F., CO2 and H2S Solubility in Acidified Aqueous Mixtures of N-Methyldiethanolamine: Experimental Measurements and Thermodynamic Modeling. *Industrial & Engineering Chemistry Research* **2025,** *64* (6), 3556-3567.

[17] Haghtalab, A.; Afsharpour, A., Solubility of $CO_2$+ $H_2S$ gas mixture into different aqueous N-methyldiethanolamine solutions blended with 1-butyl-3-methylimidazolium acetate ionic liquid. *Fluid Phase Equilibria* **2015,** *406*, 10-20.

[18] Rebolledo-Libreros, M. a. E.; Trejo, A., Gas solubility of $CO_2$ in aqueous solutions of N-methyldiethanolamine and diethanolamine with 2-amino-2-methyl-1-propanol. *Fluid Phase Equilibria* **2004,** *218* (2), 261-267.

[19] Haghtalab, A.; Izadi, A.; Shojaeian, A., High pressure measurement and thermodynamic modeling the solubility of $H_2S$ in the aqueous N-methyldiethanolamine+2-amino-2-methyl-1-propanol+piperazine systems. *Fluid Phase Equilibria* **2014,** *363*, 263-275.

[20] MacKay, D. J. C., A practical Bayesian framework for backpropagation networks. Neural Computation, **1992**, 4(3), 448-472.

[21] Burden, F.; Winkler, D., Bayesian regularization of neural networks. Methods Mol Biol. **2008**, 458, 25-44.

**Appendix A.** The ranges of the collected dataset for the ANN model.

| No. | Absorbent | Wt % | Temperature (K) | Pressure (KPa) | $H_2S$ Solubility (mol $H_2S$ / mol absorbent) | Reference |
|---|---|---|---|---|---|---|
| 1. | MDEA | 35 | 313.15 | 0.00183-313 | 0.0041-1.077 | [14] |
| | | 35 | 373.15 | 0.551-301.7 | 0.021-0.548 | [14] |
| | | 20.9 | 313.15 | 0.52-1600 | 0.13-1.725 | [15] |
| | | 50 | 323.15 | 0.1-1130.9 | 0.013-1.132 | [16] |
| | | 50 | 353.15 | 0.1-318.2 | 0.011-0.406 | [16] |
| 2. | 48.5wt% MDEA+2.66$H_2SO_4$ | 51.16 | 353.15 | 0.9-1473.8 | 0.009-0.967 | [16] |
| | | 51.16 | 323.15 | 0.1-1500.9 | 0.003-1.138 | [16] |
| 3. | 48.5%MDEA+5.21 wt%$H_2SO_4$ | 54.01 | 323.15 | 0.1-20.4 | 0.002-0.251 | [16] |
| | | 53.71 | 353.15 | 0.1-122.8 | 0.002-0.361 | [16] |
| 4. | 50wt%MDEA+(BMIM)(AC)50wt% | 100 | 348.15 | 25.45-107.98 | 0.03017-0.36049 | [17] |
| | | 100 | 323.15 | 3.27-166.09 | 0.03802-0.23937 | [17] |
| 5. | 30wt%MDEA+(BMIM)(AC)10wt% | 40 | 348.15 | 15.9-408.31 | 0.13628-0.33105 | [17] |
| | | 40 | 323.15 | 32.15-459.45 | 0.16611-0.35833 | [17] |
| 6. | 30wt%MDEA+(BMIM)(AC)5wt% | 35 | 348.15 | 44.19-423.51 | 0.14341-0.37790 | [17] |
| | | 35 | 323.15 | 44.16-473.73 | 0.20524-0.38552 | [17] |
| 7. | 50wt%MDEA+(BMIM)(AC)10wt% | 60 | 348.15 | 22.07-288.09 | 0.08579-0.28079 | [17] |
| | | 60 | 323.15 | 24.58-415.04 | 0.13602-0.31570 | [17] |
| 8. | 32.5wt%MDEA+12.5wt%DEA+6wt%AMP | 51 | 313.15 | 5.8-872 | 0.338-1.184 | [18] |
| | | 51 | 343.15 | 7.6-1004.9 | 0.349-1.106 | [18] |
| | | 51 | 393.15 | 47.9-1036.8 | 0.081-0.689 | [18] |
| 9. | 50wt%MDEA+(BMIM)(AC)5wt% | 55 | 323.15 | 24.84-437.2 | 0.17309-0.36446 | [17] |
| | | 55 | 348.15 | 39.71-371.67 | 0.10825-0.32619 | [17] |
| 10. | 25wt%MDEA+20wt%AMP | 45 | 313.15 | 294-1738 | 0.483-1.144 | [19] |
| | | 45 | 328.15 | 286-1761 | 0.48-1.088 | [19] |
| | | 45 | 343.15 | 287-1775 | 0.438-1.022 | [19] |
| 11. | 25Wt%MDEA+15wt%AMP+5wt%Pz | 45 | 313.15 | 428-1986 | 0.447-1.257 | [19] |
| | | 45 | 328.15 | 453-1975 | 0.434-1.177 | [19] |
| | | 45 | 343.15 | 434-2040 | 0.445-1.126 | [19] |
| 12. | 25wt%MDEA+10wt%AMP+10wt%Pz | 45 | 313.15 | 415-1991 | 0.396-1.264 | [19] |
| | | 45 | 328.15 | 426-2029 | 0.383-1.189 | [19] |
| | | 45 | 343.15 | 427-2047 | 0.395-1.135 | [19] |
| 13. | 25wt%MDEA+5wt%AMP+15wt%Pz | 45 | 313.15 | 213-1926 | 0.169-1.191 | [19] |
| | | 45 | 328.15 | 388-1933 | 0.287-1.11 | [19] |
| | | 45 | 343.15 | 336-1993 | 0.287-1.146 | [19] |
| 14. | 32.5wt%MDEA+12.5wt%DEA | 45 | 343.15 | 14.3-999.1 | 0.196-1.181 | [18] |
| | | 45 | 313.15 | 15.5-1021.1 | 0.404-1.226 | [18] |
| | | 45 | 393.15 | 66.1-1035.8 | 0.102-0.755 | [18] |
| 15. | 32.5wt%MDEA+12.5wt%DEA+4wt%AMP | 49 | 313.15 | 2.5-846.2 | 0.29-1.154 | [18] |
| | | 49 | 343.15 | 2.9-931.3 | 0.311-1.096 | [18] |
| | | 49 | 393.15 | 48.9-981.3 | 0.081-0.681 | [18] |
| 16. | 32.5wt%MDEA+12.5wt%DEA+10wt%AMP | 55 | 313.15 | 8.6-937.2 | 0.320-1.146 | [18] |
| | | 55 | 343.15 | 2.9-1014.5 | 0.331-1.119 | [18] |
| | | 55 | 393 | 27.8-1031.0 | 0.078-0.679 | [18] |
| 17. | 20.9wt%MDEA+ 30.5wt%Sulfolane | 51.4 | 313.15 | 1.3-1470 | 0.098-2.073 | [15] |
| | | 51.4 | 373.15 | 1.58-3210 | 0.024-1.887 | [15] |